VIP Organic Solar Cells

DOI: 10.1002/anie.201103782

Enhanced Performance and Stability of a Polymer Solar Cell by Incorporation of Vertically Aligned, Cross-Linked Fullerene Nanorods**

Chih-Yu Chang, Cheng-En Wu, Shih-Yung Chen, Chaohua Cui, Yen-Ju Cheng, Chain-Shu Hsu, Yuh-Lin Wang,* and Yongfang Li*

Research on polymer solar cells (PSC) using organic p-type (donor) and n-type (acceptor) semiconductors has attracted tremendous scientific and industrial interest in recent years.[1,2] The charge generation and charge transport play equally important roles in determining the device efficiency. To dramatically increase the area of the donor–acceptor interface for efficient charge separation, a bulk heterojunction (BHJ) is adopted to form an interpenetrating network of donor and acceptor materials.[1,2] This configuration decreases the distance that excitons need to travel to reach the heterojunction interface, thus reducing exciton recombination. However, the donor and acceptor are randomly interspersed; pathways for charges to reach the electrodes through the active layer are disordered. Free charges are likely to encounter an opposite charge, resulting in charge recombination and reduced current.[1,3,4] Moreover, space charge may be built up if charges are locally trapped on isolated domains.[5,6] Furthermore, an increase in the thickness of the BHJ layer to enhance absorption is usually accompanied by deteriorated charge collection.[7,8] Consequently, controlling phase separation toward optimal morphology in BHJ by external treatments, such as thermal or solvent annealing,[9,10] is an important but challenging task.[11]

To provide a direct path for charge transport while maintaining a large interfacial area, the ideal architecture of the donor and acceptor is the periodic, vertically aligned, and interpenetrating ordered bulk heterojunction (OBHJ).[1,12–14] The electrons and holes have straight and independent pathways to the electrodes to shorten the carrier transport length and reduce the probability of charge recombination. Several elegant studies have attempted to demonstrate this conceptual architecture, for example by a template-assisted strategy or self-assembly of block copolymer.[11,14–16] However, realization of high-performance OBHJ devices has not been successful. We envision that designing a system that combines a BHJ for efficient charge generation with an OBHJ for efficient charge transport and collection would be a more practical strategy. Such a configuration is specifically suitable for solar cells with inverted architecture, because an electron-selective layer is required at the bottom of the active layer for electron extraction and hole blocking.[17] For instance, the upper BHJ active layer of an inverted solar cell is infiltrated into vertically aligned nanorods extending from a bottom layer of an inorganic semiconductor (e.g. ZnO or TiO_2).[18–20] However, owing to the poor electrical coherence at the organic/inorganic interface,[20,21] the improvement in efficiency is moderate (PCE ranges from 2.1 to 2.7%).

Recently, we reported a cross-linkable fullerene material, [6,6]-phenyl-C_{61}-butyric styryl dendron ester (PCBSD). The formation of a cross-linked PCBSD (C-PCBSD, Figure 1a) planar layer allows realization of a multilayer inverted device by all-solution processing.[22] By using indene–C_{60} bisadduct (ICBA, Figure 1a) with a higher-lying lowest unoccupied molecular orbital (LUMO) energy level to serve as the acceptor in the blend, an inverted solar cell device based on the ITO/ZnO/C-PCBSD/ICBA:P3HT/PEDOT:PSS/Ag configuration achieved an enhanced power conversion efficiency

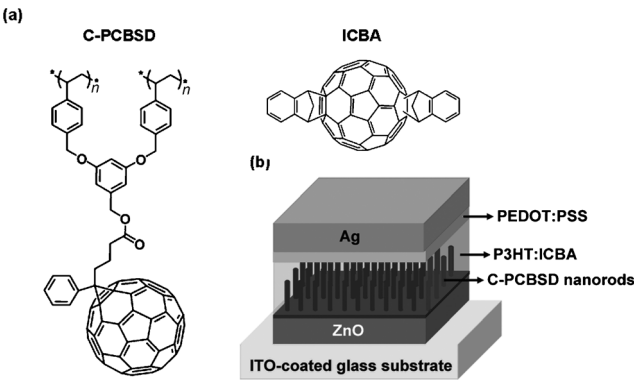

Figure 1. a) Chemical structure of C-PCBSD and ICBA. b) Schematic representation of the nanostructured device architecture used in this study. PEDOT = poly(3,4-ethyldioxythiophene), PSS = poly(styrene sulfonate), P3HT = poly(3-hexylthiophene), ITO = indium tin oxide.

[*] Dr. C.-Y. Chang, C.-E. Wu, Prof. Y.-J. Cheng, Prof. C.-S. Hsu, Prof. Y.-L. Wang
Department of Applied Chemistry, National Chiao Tung University
Hsin-Chu 30010 (Taiwan)
E-mail: cshsu@mail.nctu.edu.tw
S.-Y. Chen
Department of Physics, National Taiwan University
Taipei 10617 (Taiwan)
and
Institute of Atomic and Molecular Science, Academia Sinica
PO Box 23-166, Taipei 10617 (Taiwan)
C. Cui, Prof. Y. Li
Beijing National Laboratory for Molecular Sciences
CAS Key Laboratory of Organic Solids, Institution of Chemistry
Chinese Academy of Sciences, Beijing 100190 (China)

[**] This work is supported by the National Science Council (NSC100-3113-E-009-005) and "ATU Plan" of Ministry of Education, Taiwan.

Supporting information for this article is available on the WWW under http://dx.doi.org/10.1002/anie.201103782.

(PCE) of 6.2%.[23] To further magnify the positive effects of C-PCBSD interlayer on the performance, we present here a new active-layer configuration where the bulk heterojunction of the P3HT:ICBA upper layer was deposited on a C-PCBSD bottom layer with vertically oriented nanorods to create a well-organized nanostructured interface (Figure 1b). The resultant device (ITO/ZnO/C-PCBSD nanorods/ICBA:P3HT/PEDOT:PSS/Ag) not only achieved an enhanced PCE of 7.3% but also exhibited exceptional ambient and morphological stability.

The anodic aluminum oxide (AAO) template-assisted approach has been widely employed to construct ordered nanostructures.[24–26] The template-assisted fabrication of arrays of free-standing C-PCBSD nanorods is schematically illustrated in Scheme 1. In detail, 1) a solution of PCBSD (20 mg mL^{-1} in 1,2-dichlorobenzene) was spin-coated on top of an AAO template (thickness ca. 90 nm, Scheme 1a); 2) a glass substrate/ITO/ZnO/ultrathin PCBSD film (thickness < 5 nm) was pressed on the top of the spin-coated AAO template and the two were laminated together (Scheme 1b); 3) the sample was placed inside a jar (capacity 15 mL) containing 1 mL 1,2-dichlorobenzene at room temperature for 24 h and then heated at 80 °C for 10 h with an applied pressure of 200 bar in a vacuum oven to induce the infiltration of PCBSD into the pores of the AAO template (Scheme 1c); 4) PCBSD was cross-linked in the confinement of the AAO template by heating at 170 °C for 1 h (Scheme 1d); 5) after the applied pressure was released and the samples were cooled back to room temperature, the AAO template was removed by treatment with 5 wt.% phosphoric acid without affecting the cross-linked PCBSD nanorods (Scheme 1e); 6) the nanostructured sample was rinsed with methanol for several times and then dried in a vacuum oven for 2 h. It should be noted that a precoated ultrathin PCBSD film used in step (2) could enhance the adhesion between the nanostructure and the ZnO-coated ITO substrate, thus avoiding the delamination problem upon removing the AAO template.

The AAO template used in this study exhibits a uniform pore size of approximately 60 nm and an interpore distance (distance between centers of two neighboring pores) of approximately 100 nm, as determined from a scanning electron microscopy (SEM) image (Figure 2a). To provide the maximum interface for exciton dissociation from C-PCBSD nanorods and to ensure complete filling of the space between the rods with the P3HT:ICBA layer, it is essential to obtain vertical nanorods without aggregation and collapses. The successful formation of highly ordered, vertical C-PCBSD nanorod arrays over large areas was evidenced by low-magnification SEM image (Figure 2b). High-magnification SEM (Figure 2c) indicated that the C-PCBSD nanorods exhibited an average pore size of approximately 60 nm and an interpore distance of 100 nm, both of which are consistent with those of the corresponding AAO template (Figure 2a). It should be noted that the enhanced robustness of the cross-linked network allows us to construct nanorods with a maximum sustainable height of up to about 80 nm. Over this height, aggregation and collapse of the nanorods into conical bundles were observable (Figure S1, Supporting Information). The structural failure is due to the capillary force exerted on the nanorods upon the evaporative drying of the solvents used for the removal of the AAO scaffold.[27] Furthermore, a solution of P3HT:ICBA in 1,2-dichlorobenzene was then successfully spin-cast on top of the solvent-resistant cross-linked nanostructure without destroying it. Finally, after deposition of PEDOT:PSS solution and subsequent vacuum evaporation of silver as the anode, the multilayer inverted solar cell device B based on the configuration ITO/ZnO/C-PCBSD nanorods/P3HT:ICBA/PEDOT:PSS/Ag was completed. Under identical fabrication conditions, a control device A, using ITO/ZnO/planar C-PCBSD/

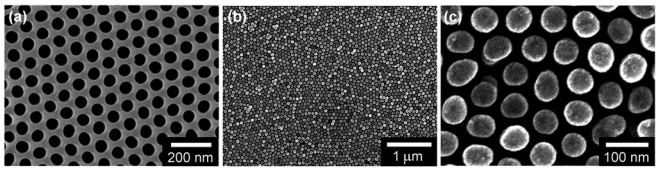

Figure 2. SEM images of a) a bare AAO template and b,c) C-PCBSD nanorods under low magnification (b) and high magnification (c).

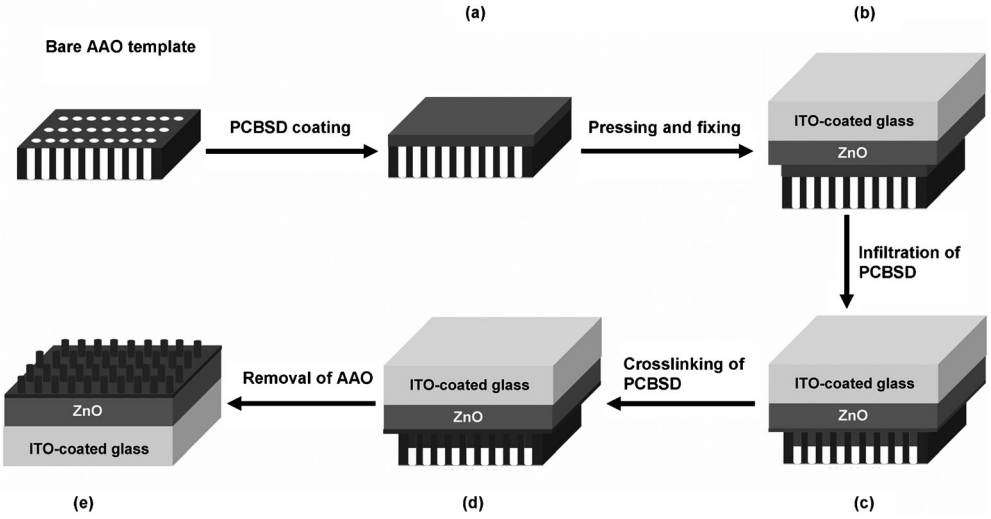

Scheme 1. Schematic diagram of the AAO template-assisted fabrication of C-PCBSD nanorods. See text for details.

P3HT:ICBA/PEDOT:PSS/Ag configuration (without the C-PCBSD nanostructure), was also fabricated for comparison. Current density–voltage (J–V) characteristics of the devices are shown in Figure 3, and the device parameters are summarized in Table 1. Under AM1.5G solar irradiation with light intensity of 100 mW cm^{-2}, device A exhibited a high PCE value of 6.2%, with an open-circuit voltage (V_{oc}) of 0.84 V, a short-circuit current density (J_{sc}) of 11.17 mA cm^{-2}, and a fill factor (FF) of 66.0%. Encouragingly, device B incorporating C-PCBSD nanorods achieved an exceptional PCE of 7.3%, with $V_{oc} = 0.84$ V, $J_{sc} = 12.07$ mA cm^{-2}, and FF = 72.3%. Note that the J_{sc} values are consistent with the values calculated from integrated incident photon-to-current conversion efficiency (IPCE) spectra (Figure S2, Supporting Information), which confirms the accuracy of our reported PCE values.

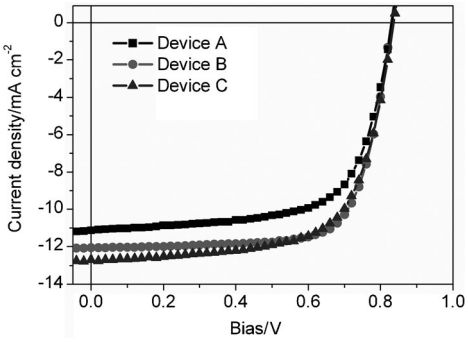

Figure 3. *J–V* characteristics of the as-fabricated devices; see Table 1 for descriptions of the device types.

Table 1: Summary of the device parameters.

Device	Conditions[a]	V_{oc} [V]	J_{sc} [mA cm^{-2}]	FF [%]	PCE [%]	Hole mobility [cm^2 V^{-1} s^{-1}]	Electron mobility [cm^2 V^{-1} s^{-1}]
A	without, 170 nm	0.84	11.17	66.0	6.2	3.1×10^{-3}	9.4×10^{-4}
B	with, 170 nm	0.84	12.07	72.3	7.3	2.8×10^{-3}	2.6×10^{-3}
C	with, 360 nm	0.84	12.70	65.1	6.9	N/A[b]	N/A[b]

[a] With or without nanorods, active layer thickness. [b] N/A = not available

Compared to the device characteristics of the control device A, the PCE improvements in the device B mainly originated from the higher J_{sc} value (Table 1 and Figure 3). This enhancement could be ascribed to the fact that the array of C-PCBSD nanorods penetrating into the BHJ layer offers substantial P3HT/C-PCBSD interfacial area for extra exciton dissociation, thereby generating a higher photocurrent. Steady-state photoluminescence (PL) measurements were performed to study the extent of exciton dissociation in the control sample (i.e. glass/ZnO/planar C-PCBSD/P3HT:ICBA) and the experimental sample (i.e. glass/ZnO/C-PCBSD nanorods/P3HT:ICBA; Figure S3, Supporting Information). A more pronounced quenching of the PL intensity was observed in the experimental sample than in the control sample, thus confirming that the exciton dissociation is more efficient in the presence of C-PCBSD nanorods. In addition to the improvement in J_{sc}, the experimental device B also exhibited a higher FF value than the control device A (72.3% vs. 66.0%, Table 1 and Figure 3), which was attributed to the improved balance between the electron and hole mobilities (i.e. a reduced space charge build-up) within the active layer. As shown in Table 1 and Figure S4 (Supporting Information), the introduction of C-PCBSD nanorods enhanced the electron mobility from 9.4×10^{-4} to 2.6×10^{-3} cm^2 V^{-1} s^{-1} while maintaining the hole mobility value of approximately 3×10^{-3} cm^2 V^{-1} s^{-1}, thus leading to more balanced charge transport (the electron-to-hole mobility ratio is 1.1). Such an enhancement in electron mobility has also been demonstrated in previous studies, showing that nanostructured organic semiconductors can possess superior charge-transport properties than their planar counterparts.[11,15,28,29]

Considering that the C-PCBSD nanostructure can facilitate efficient carrier transport and collection, increasing the thickness of the active layer to 360 nm (device C) did not cause significant deterioration in the PCE, overcoming the trade-off between absorption and charge transport. As shown in Table 1 and Figure 3, compared with device B, device C exhibited an enhanced J_{sc} of 12.7 mA cm^{-2} and a slightly reduced FF of 65%, leading to a comparable PCE of 6.9%. This thickness-independent property is beneficial for mass production techniques, such as roll-to-roll fabrication.

The air-stability of the experimental device B without encapsulation was evaluated by monitoring the evolution of the PCE as a function of time upon storage in ambient air (Figure 4). Device B retained over 90% of its initial PCE value after being exposed to ambient conditions for 450 h. Inverted device B exhibits not only excellent air stability but also superior long-term thermal stability to the control device A (Figure 4). When stored in inert atmosphere at elevated temperature (100 °C), the control device A had a half life (defined as the time period for the PCE to decay to 50% of the initial value) of 220 h, while the experimental device B had a much improved half life of more than 689 h (Figure 4). The more significant reduction in efficiency observed in the control device A is associated with its macrographic alteration of the morphology, which was witnessed by optical microscopy (Figure S5,

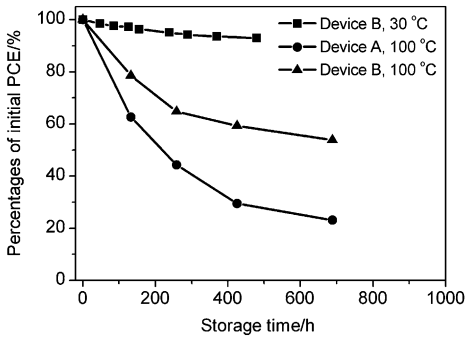

Figure 4. Degradation profiles of unencapsulated devices stored at either 30 °C in ambient air or at 100 °C in the glove box.

Supporting Information). After heating the samples at 100 °C for 689 h, the control sample showed the formation of dense, needle-shaped ICBA clusters, whereas less dense ICBA clusters were observed in the experimental sample. Considering that a part of the P3HT:ICBA BHJ infiltrated into the C-PCBSD nanorods and is thus surrounded and confined between the rods on a scale of approximately 40 nm (determined by the edge-to-edge distance between the pores shown in the SEM image, Figure 2a), nanostructure-assisted morphological stability could be rationalized by the spatial confinement effect, which might suppress the thermal-driven crystallization of ICBA and P3HT upon thermal annealing.

In conclusion, we have successfully utilized an AAO template-assisted strategy in combination with a cross-linking approach to construct an array of robust and well-organized C-PCBSD nanorods. A P3HT:ICBA BHJ upper layer was deposited on the C-PCBSD bottom layer with the vertically aligned nanorods to create an organic/organic ordered nanostructured heterojunction. Owing to the enhanced charge generation and straight electron transport pathways, the inverted solar cell incorporating C-PCBSD nanorods achieved a record high PCE of 7.3%, which is the highest value ever reported for P3HT:fullerene-based BHJ solar cells.

Experimental Section

Preparation of AAO templates: High-purity (99.99%) annealed Al substrates were electropolished in a mixture $HClO_4$ and C_2H_5OH (1:5 vol/vol) until the root-mean-square surface roughness of a typical 10 μm × 10 μm area was 1 nm, as measured by contact-mode atomic force microscopy. The polished Al substrate was anodized at 40 V in 2 °C oxalic acid (0.3 M) for 5 h to grow AAO, which was then removed by a solution of CrO_3 (1.5 g) and 6% H_3PO_4 at 70 °C in 3.5 h. The Al substrate was anodized again under the same conditions for 10 h to grow AAO. After dissolving the remaining Al underneath by a solution of $CuCl_4$ (2 wt%) in HCl (37.5 wt.%, 50 mL) in 20 min, the resulting AAO template was etched in 5% H_3PO_4 solution at 40 °C for 40 min to remove its barrier oxide layer and widen its pores simultaneously.

The device fabrication procedure was follows: 1) ultrasonication in acetone for 20 min and subsequent rinsing with deionized water; 2) ultrasonication in isopropyl alcohol for 20 min and subsequent rinsing with deionized water; 3) UV/ozone treatment for 20 min; 4) spin casting of the ZnO precursor from zinc acetylacetonate hydrate (purchased from Aldrich and used as received) in methanol (20 mg mL^{-1}) and subsequent baking at 130 °C for 10 min in air (thickness 20 nm); 5) spin-casting of PCBSD solution (7 mg mL^{-1} in 1,2-dichlorobenzene) on top of the ZnO layer (thickness ca. 10 nm); 6) spin-casting of the active layer from a 1,2-dichlorobenzene solution of P3HT (17 mg mL^{-1}, MW = 50000 g mol^{-1}, purchased from Rieke Metals and used as received) and ICBA (17 mg mL^{-1}, provided by ICCAS and used as received), and subsequent drying of the films at room temperature in a closed Petri dish overnight (thickness 170 nm); 7) spin-casting of the PEDOT:PSS layer from Clevios P (H. C. Starck) diluted with equal volume of 2-propanol and 0.2 wt.% polyoxyethylene-6-tridecylether (Aldrich) at subsequent baking at 60 °C for 10 min (thickness 60 nm); 8) thermal evaporation of the Ag layer under high vacuum ($< 10^{-6}$ Torr; thickness = 200 nm) through a shadow mask which defined an active area of 0.04 cm^2; 9) thermal annealing of the complete device at 150 °C for 7 min.

Characterization: the J–V characteristics of the PSC devices were measured with a Keithley 2400 source meter under simulated AM1.5G illumination (SAN-EI XES-301S solar simulator with integrated intensity of 100 mW cm^{-2}), which was calibrated with a Hamamatsu silicon photodiode with KG-5 filter against an NREL-calibrated solar simulator.[30] IPCE spectra were measured using a lock-in amplifier with a current preamplifier under short-circuit conditions with illumination of monochromatic light from a 250 W quartz-halogen lamp (Osram) passing through a monochromator (Spectral Products CM110). SEM was conducted with a field-emission SEM instrument (JSM-7401F, JEOL) operated at an accelerating voltage of 10 kV with the samples coated with approximately 3 nm platinum. The PL spectrum was recorded with Hitachi F-4500 spectrophotometer equipped with a 150 W xenon lamp at room temperature. Optical microscopy images were recorded with Nikon optical microscope (E5000m1) at room temperature. The single-carrier mobility can be extracted from the dark *J–V* characteristics of the hole-only and electron-only devices by using space charge limited current (SCLC) model.[31,32] The hole-only device was constructed as ITO/Au (40 nm)/MoO_3 (10 nm)/C-PCBSD interlayer/with or without C-PCBSD nanorods/P3HT:ICBA/PEDOT:PSS/Ag, and the electron-only device was constructed as ITO/ZnO/C-PCBSD interlayer/with or without C-PCBSD nanorods/P3HT:ICBA/Ca (10 nm)/Al (100 nm). The fabrication procedure was identical to that of solar cell fabrication except for the electrodes.

Received: June 3, 2011
Published online: August 22, 2011

Keywords: device stability · nanostructures · organic photovoltaics · polymers · solar cells

[1] K. M. Coakley, M. D. McGehee, *Chem. Mater.* **2004**, *16*, 4533–4542.
[2] S. Günes, H. Neugebauer, N. S. Sariciftci, *Chem. Rev.* **2007**, *107*, 1324–1338.
[3] X. He, F. Gao, G. Tu, D. Hasko, S. Hüttner, U. Steiner, N. C. Greenham, R. H. Friend, W. T. S. Huck, *Nano Lett.* **2010**, *10*, 1302–1307.
[4] H. Hoppe, N. S. Sariciftci, *Adv. Polym. Sci.* **2008**, *214*, 1–86.
[5] L. J. A. Koster, V. D. Mihailetchi, P. W. M. Blom, *Appl. Phys. Lett.* **2006**, *88*, 052104.
[6] I. Hwang, C. R. McNeill, N. C. Greenham, *J. Appl. Phys.* **2009**, *106*, 094506.
[7] G. Li, V. Shrotriya, Y. Yao, Y. Yang, *J. Appl. Phys.* **2005**, *98*, 1–5.
[8] C. Zhang, S. W. Tong, C. Jiang, E. T. Kang, D. S. H. Chan, C. Zhu, *Appl. Phys. Lett.* **2008**, *93*, 043307.
[9] W. Ma, C. Yang, X. Gong, K. Lee, A. J. Heeger, *Adv. Funct. Mater.* **2005**, *15*, 1617–1622.
[10] G. Li, V. Shrotriya, J. Huang, Y. Yao, T. Moriarty, K. Emery, Y. Yang, *Nat. Mater.* **2005**, *4*, 864–868.
[11] J. S. Kim, Y. Park, D. Y. Lee, J. H. Lee, J. H. Park, J. K. Kim, K. Cho, *Adv. Funct. Mater.* **2010**, *20*, 540–545.
[12] M. D. McGehee, *MRS Bull.* **2009**, *34*, 95–100.
[13] T. Sagawa, S. Yoshikawa, H. Imahori, *J. Phys. Chem. Lett.* **2010**, *1*, 1020–1025.
[14] C. Y. Kuo, W. C. Tang, C. Gau, T. F. Guo, D. Z. Jeng, *Appl. Phys. Lett.* **2008**, *93*, 033307.
[15] J. I. Lee, S. H. Cho, S. M. Park, J. K. Kim, J. W. Yu, Y. C. Kim, T. P. Russell, *Nano. Lett.* **2008**, *8*, 2315–2320.
[16] J. Weickert, R. B. Dunbar, H. C. Hesse, W. Wiedemann, L. Schmidt-Mende, *Adv. Mater.* **2011**, *23*, 1810–1828.
[17] L. M. Chen, Z. Hong, G. Li, Y. Yang, *Adv. Mater.* **2009**, *21*, 1434–1449.
[18] K. Takanezawa, K. Hirota, Q. S. Wei, K. Tajima, K. Hashimoto, *J. Phys. Chem. C* **2007**, *111*, 7218–7223.

[19] M. Wang, Y. Li, H. Huang, E. D. Peterson, W. Nie, W. Zhou, W. Zeng, W. Huang, G. Fang, N. Sun, X. Zhao, D. L. Carroll, *Appl. Phys. Lett.* **2011**, *98*, 103305.
[20] C. T. Chen, F. C. Hsu, S. W. Kuan, Y. F. Chen, *Sol. Energy Mater. Sol. Cells* **2011**, *95*, 740 – 744.
[21] C. Goh, S. R. Scully, M. D. McGehee, *J. Appl. Phys.* **2007**, *101*, 114503.
[22] C. H. Hsieh, Y. J. Cheng, P. J. Li, C. H. Chen, M. Dubosc, R. M. Liang, C. S. Hsu, *J. Am. Chem. Soc.* **2010**, *132*, 4887 – 4893.
[23] Y. J. Cheng, C. H. Hsieh, Y. He, C. S. Hsu, Y. Li, *J. Am. Chem. Soc.* **2010**, *132*, 17381 – 17383.
[24] H. H. Wang, C. Y. Liu, S. B. Wu, N. W. Liu, C. Y. Peng, T. H. Chan, C. F. Hsu, J. K. Wang, Y. L. Wang, *Adv. Mater.* **2006**, *18*, 491 – 495.
[25] N. W. Liu, C. Y. Liu, H. H. Wang, C. F. Hsu, M. Y. Lai, T. H. Chuang, Y. L. Wang, *Adv. Mater.* **2008**, *20*, 2547 – 2551.
[26] K. T. Tsai, Y. R. Huang, M. Y. Lai, C. Y. Liu, H. H. Wang, J. H. He, Y. L. Wang, *J. Nanosci. Nanotechnol.* **2010**, *10*, 8293 – 8297.
[27] G. Chen, S. A. Soper, R. L. McCarley, *Langmuir* **2007**, *23*, 11777 – 11781.
[28] A. Santos, P. Formentín, J. Pallarés, J. Ferré-Borrull, L. F. Marsal, *Sol. Energy Mater. Sol. Cells* **2010**, *94*, 1247 – 1253.
[29] F. S. Kim, G. Ren, S. A. Jenekhe, *Chem. Mater.* **2011**, *23*, 682 – 732.
[30] V. Shrotriya, G. Li, Y. Yao, T. Moriarty, K. Emery, Y. Yang, *Adv. Funct. Mater.* **2006**, *16*, 2016 – 2023.
[31] M. F. Falzon, M. M. Wienk, R. A. J. Janssen, *J. Phys. Chem. C* **2011**, *115*, 3178 – 3187.
[32] V. D. Mihailetchi, H. Xie, B. De Boer, L. J. A. Koster, P. W. M. Blom, *Adv. Funct. Mater.* **2006**, *16*, 699 – 708.

